Vasculature and flow in microfluidic systems

Kramer, B.

Chapter 3

3D human microvessel-on-a-Chip model for studying monocyte-to-endothelium adhesion under flow – application in systems toxicology

Carine Poussin*, Bart Kramer*, Henriette L. Lanz*, Angelique van den Heuvel, Alexandra Laurent, Thomas Olivierb, Marjolein Vermeer, Dariusz Peric, Karine Baumer, Rémi Dulize, Emmanuel Guedj, Nikolai V. Ivanov, Manuel C. Peitsch, Julia Hoeng, and Jos Joore

Published in: Alternatives for Animal Experimentation (2020) 37

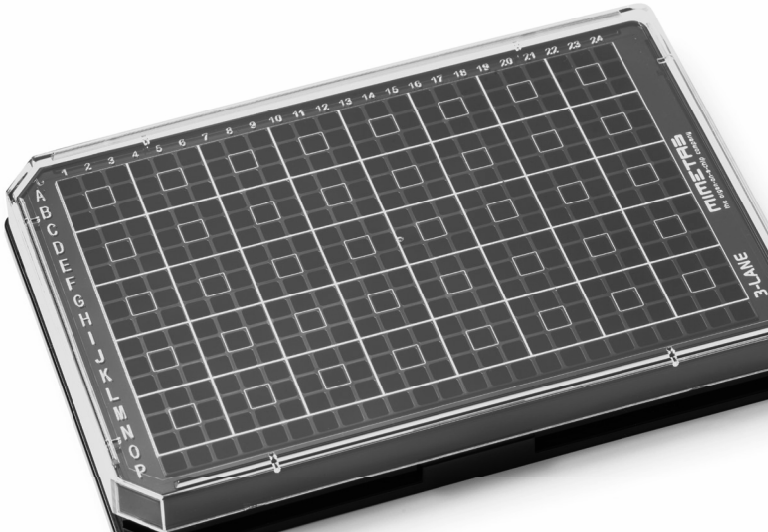

Abstract

Lifestyle and genetic factors can lead to the development of atherosclerosis and, ultimately, cardiovascular adverse events. Rodent models are commonly used to investigate mechanism(s) of atherogenesis. However, the 3Rs principles, aiming to limit animal testing, encourage the scientific community to develop new physiologically relevant in vitro alternatives. Leveraging the 96-chip OrganoPlate®, a microfluidic platform, we have established a three-dimensional (3D) model of endothelial microvessels-on-a-chip under flow using primary human coronary arterial endothelial cells. As functional readout, we have set up an assay to measure the adhesion of monocytes to the lumen of perfused microvessels. For monitoring molecular changes in microvessels, we have established the staining and quantification of specific protein markers of inflammation and oxidative stress using high content imaging, as well as analyzed transcriptome changes using microarrays. To demonstrate its usefulness in systems toxicology, we leveraged our 3D vasculature-on-a-chip model to assess the impact of the Tobacco Heating System (THS) 2.2, a candidate modified risk tobacco product, and the 3R4F reference cigarette on the adhesion of monocytic cells to endothelial microvessels. Our results show that THS 2.2 aerosol-conditioned medium had a reduced effect on monocyte-endothelium adhesion compared with 3R4F smoke-conditioned medium. In conclusion, we have established a relevant 3D vasculature-on-a-chip model for investigating leukocyte-endothelial microvessel adhesion. A case study illustrates how the model can be used for product testing in the context of systems toxicology-based risk assessment. The current model and its potential further development options also open perspectives of applications in vascular disease research and drug discovery.

Introduction

The endothelium is a single layer of cells at the interface between circulating blood and organ tissues that plays critical roles in vascular processes, such as barrier permeability,[1] vasotone regulation, leukocyte adhesiveness and extravasation, blood clotting, and angiogenesis.[2] Endothelial dysfunction that increases permeability, adhesiveness, and transmigration of leukocytes as well as the accumulation of fatty streaks in the subendothelial compartment[3] are a hallmark of atherosclerosis, characterized by the development of plaques that can become unstable and rupture, resulting in cardiovascular adverse events.[2]

The development of atherosclerosis and its prevention by therapeutic interventions is studied extensively in humans and in rodent models. Although highly relevant, the use of in vivo models remains technically challenging for in-depth and rapid mechanistic investigations, such as the deconvolution of the effects on endothelial cells of different molecules present in a milieu. Moreover, the identification of potent drug compounds for therapeutic intervention and the testing of compounds/products for toxicological safety or risk assessments require high-throughput settings for a pre-screening phase that is generally not conducted in vivo. The perspective of the 3Rs principle, "replacement, reduction,

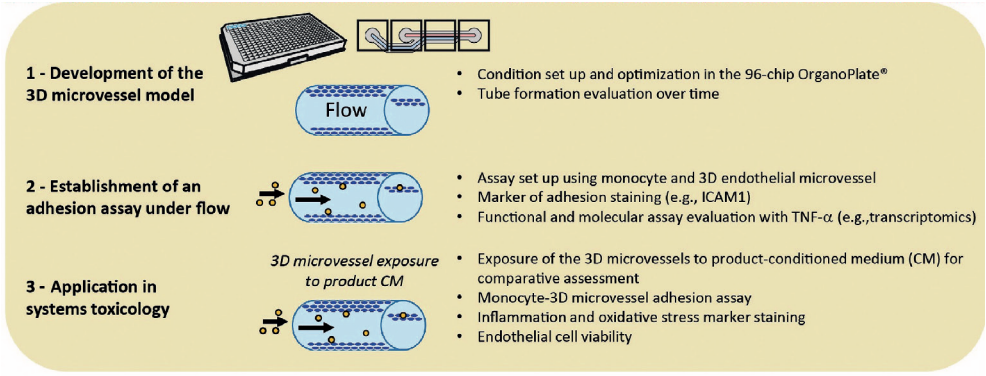

Figure 1. Overview of the steps for the development, functional evaluation, and real-case application in systems toxicology of our 3D vasculature-on-a-chip model for studying monocyte-endothelial adhesion under flow.

and refinement," which aims to limit animal testing,[4] encourages the scientific community to develop relevant in vitro alternatives. So far, two-dimensional (2D) and static endothelial in vitro models have been used extensively, but more physiologically relevant models are required that integrate the three-dimensional (3D) geometry of vessels and hemodynamic flow. These properties play important mechanical roles through mechano-transduction signaling that influence vascular differentiation and proliferation as well as endothelial cell morphology and response to stimuli.[5,6] Along with other factors, flow patterns and the magnitude of shear stress promote anti- or pro-atherogenic effects on endothelial cells that contribute to the protection or promotion of vascular diseases.[6,7]

The emergence of a wide range of engineered microfluidic systems and techniques enabling the culture of cells under flow and in a 3D space has accelerated the innovation of advanced perfusable in vitro vascular models. These models vary in complexity and physiological relevance, from a simple planar endothelial cell layer, on top of which controlled shear stress can be applied, to 3D microvessels or even more complex vasculature networks.[8,9] Models are classified according to their method of fabrication and constitute a toolbox for studying different aspects of vascular biology.[9] Each model offers advantages (e.g., high physiological relevance, high-throughput capacity, easy setup) and possesses limitations (e.g., time-consuming to manufacture, low throughput, lower physiological relevance).[9] Therefore, it is important to define the biological mechanism(s) of interest, the extension potential of the model, and the capacity needed to select or develop a vascular model that adequately balances experimental feasibility, physiological relevance, and throughput capacity for larger experimental condition screening.

Lifestyle and genetic predisposition affect the development of vascular disorders that result in atherogenesis.[10] Smoking, for instance, is a recognized major risk factor for the development of cardiovascular diseases.[11] Over time, smokers develop low-grade inflammation and oxidative properties in the systemic compartment that can alter endothelial function, resulting in the initiation and

progression of atherosclerosis.[12] The health risks associated with cigarette smoking are attributable to toxicants that are generated in the smoke through tobacco combustion.[13] Therefore, reducing exposure to smoke constituents is crucial for risk reduction,[14] for which the development of modified risk tobacco products (MRTP) is necessary.[15] Potential MRTPs that heat tobacco rather than burning it have been developed, offering significant decreases in the complexity and number of toxicants generated in the aerosol during use.[16] Pre-clinical and clinical studies aimed to assess these products have compared them with cigarettes to determine whether this reduction in exposure translates into a reduction in health risk in both laboratory models and humans.[14] Overall, the results indicated that the Tobacco Heating System (THS) 2.2, a candidate MRTP, and the Carbon-Heated Tobacco Product (CHTP) 1.2, a potential MRTP, exert reduced effects on respiratory and cardiovascular functional and molecular endpoints in both in vitro and in vivo laboratory models.[17–20] Human studies showed significant reduction in biomarkers of exposure and potential harm after switching from cigarettes to THS 2.2.[21]

The present work aimed to develop a 3D vasculature-on-a-chip model under flow to study monocyte-endothelium adhesion and provide a use case application by leveraging this model for tobacco product testing in a systems toxicology framework (Figure 1). Using the OrganoPlate®, a standardized 96-chip microfluidic cell culture plate, we optimized conditions to grow endothelial microvessels with disease-relevant primary human coronary artery endothelial cells (HCAEC, Figure 1, Step 1). This microfluidic platform has been used previously to develop perfusable human umbilical vein endothelial cells, VeraVec human endothelial cell vessels, for studying vascular permeability.[8] To evaluate the functionality and relevance of the HCAEC microvessel model, we developed an assay to quantify (i) the adhesion of monocytic cells under flow to the lumen of HCAEC microvessels as a functional readout and (ii) the intercellular adhesion molecule 1 (ICAM1; also known as CD54) protein in HCAECs as a molecular readout for adhesion (Figure 1, Step 2). We used tumor necrosis factor α (TNFα), a prototypical inflammatory

stimulus known to trigger monocyte-endothelium adhesion, and also investigated concentration-dependent gene expression changes in HCAEC microvessels using transcriptomics. As a real-case application of our 3D vasculature-on-a-chip model, we assessed the comparative impact of THS 2.2 aerosol and 3R4F cigarette smoke in the form of conditioned medium on the adhesion of monocytic cells to HCAEC microvessels, a key event in atherogenesis (Figure 1, Step 3). After exposure to conditioned medium, glutathione (GSH) content was also measured to quantify oxidative stress promoted in endothelial microvessels similarly to smokers' blood that acquired oxidative properties over time and may contribute to endothelial dysfunction.[22]

Material and methods

Cell culture

Primary HCAECs (PromoCell 12221; Heidelberg, Germany) were cultured in pre-coated tissue culture flasks (Nunc Easyflask; Roskilde, Denmark) with MV2 endothelial cell growth medium (PromoCell C-22-22) containing 5% fetal bovine serum (FBS, Gibco 16140-071; Waltham, MA, USA) and 1% penicillin/streptomycin (Sigma-Aldrich P4333; St. Louis, MO, USA). Mono-Mac-6 (MM6) cells (DSMZ, ACC-No.124; Braunschweig, Germany) were maintained in Roswell Park Memorial Institute (RPMI) 1640 medium (Sigma-Aldrich R0883) containing 10% FBS and 1% penicillin/streptomycin.

OrganoPlate® culture

We used two-lane OrganoPlates® with 400 µm × 220 µm (w × h) channels (MIMETAS 9603-400B, Leiden, The Netherlands). Gel and perfusion channel lengths were 9 mm and 12.2 mm, respectively. Before seeding, 50 µL of Hank's Balanced Salt Solution (HBSS) were dispensed into the observation window to

prevent evaporation and enhance optical clarity. Two microliters of gel composed of 4 mg/mL collagen I (Cultrex rat collagen 1, 5 mg/mL; Trevigen, Gaithersburg, MD, USA), 100 mM HEPES (Gibco 15630-056), and 3.7 mg/mL Na2HCO3 (Sigma-Aldrich S5761) were dispensed in the gel inlet and incubated for 30 minutes at 37 °C allowing gelation of the extracellular matrix (ECM). HCAECs at passage three were trypsinized using 0.025% trypsin in phosphate-buffered saline (PBS)/ethylenediaminetetraacetic acid (Lonza CC-5012; Basel, Switzerland) and resuspended in the appropriate volume (106 cells/mL) in MV2 medium. Two microliters of cell solution were dispensed in the perfusion channel inlet of the OrganoPlate®. After addition of the cells, 50 µL of MV2 medium were dispensed in the perfusion inlet to prevent dehydration of the cell suspension. The plate was incubated on its side for two hours to allow the cells to attach to the ECM. Subsequently, 50 µL of MV2 medium were dispensed in the perfusion outlet, and the plate was placed in the incubator (37 °C, 5% CO2) on a rocking platform (four-minute intervals at an angle of 7°) resulting in a bidirectional flow. For the culture optimization step, we used 9.1 mg/mL of Matrigel growth factor reduced basement membrane matrix (Corning 356231; Corning, NY, USA) and endothelial medium from Cell Biologics (H1168; Chicago, IL, USA). ECM and medium were mixed at a 1:1 (v/v) ratio. The medium was changed three times per week.

Barrier integrity assay

Medium in the perfusion channel was replaced by MV2 medium containing 0.5 mg/mL 20 kDa fluorescein isothiocyanate (FITC)-dextran (Sigma-Aldrich FD20S) and 0.5 mg/mL 155 kDa tetramethylrhodamine isothiocyanate (TRITC)-dextran (Sigma-Aldrich T1287) (40 µL on perfusion inlet, 30 µL on perfusion outlet). Ten microliters of MV2 medium were dispensed on the gel inlet. Leakage of the fluorescent probe from the lumen of the endothelial microvessel into the ECM compartment was captured using an ImageXpress XLS Micro HCI system (two-minute intervals, 14 minutes total; Molecular Devices, San Jose, CA, USA). The ratio between the fluorescent signal in the perfusion channel and the ECM channel

was analyzed using Fiji (ImageJ, NIH, Bethesda, MD, USA). The permeability of the membranes was analyzed by measuring the number of molecules that leaked though the membrane into the adjacent gel lane over time. From these measurements, the apparent permeability index (Papp: initial flux of a compound through a membrane, normalized by membrane surface area and donor concentration) was calculated using the following formula:

$$P_{app} = \frac{\triangle C_{receiver} \times V_{receiver}}{\triangle t \times A_{barrier} \times C_{donor}} \left(\frac{cm}{s} \right)$$

where $\Delta C_{receiver}$ is the measured normalized intensity difference of the ECM to the donor channel at t_{0min} and t_{10min}, Vreceiver is the volume of the measured region in the ECM channel, Δt is the time difference, $A_{barrier}$ is the surface of the ECM interface with the medium channel, and C_{donor} is the donor concentration of the dextran dye (0.5 mg/mL).

Monocyte-endothelial microvessel adhesion assay under flow

MM6 monocytes (passage 12) were harvested and suspended at a density of 105 cells/mL in RPMI medium containing 0.5 µg/mL calcein AM (Life Technologies C3099; Carlsbad, CA, USA) for 15 minutes at 37 °C. The monocytes were spun down at 200 × g for five minutes, the calcein AM-containing medium was aspirated, and the cells were resuspended in a density of 105 cells/mL in MV2 medium. Simultaneously, the nuclei of the endothelial microvessels were stained with Hoechst 33342 (1:2,000, Thermo Fisher Scientific H3570; Waltham, MA, USA) for 20 minutes at 37 °C. After washing the endothelial tube for five minutes with MV2 medium, the monocyte suspension was added to the perfusion channel and incubated at 37 °C and 5% CO2 for 15 minutes on a rocking platform (eight-minute intervals at a 7° angle). After washing twice with HBSS for five minutes, the endothelial vessel was imaged using an ImageXpress XLS-C HCI system. The number of endothelial nuclei in the microvessels was extracted using an approach based on morphological shape filtering using built-in tools available in Fiji (version

2) / ImageJ (1.52e build).[23] Endothelial cells nuclei were extracted by removing the background signal via a Rolling Ball method in the blue Hoechst channel.[24] After the remaining signal was thresholded to highlight the nuclei, a particle detection was subsequently performed to count the number of nuclei. The number of adhering monocytes was extracted using methods based on intensity thresholding and particle detection in the green calcein AM channel.[25] The method used was nearly identical to the method described for obtaining the number of endothelial nuclei. The expected minimum size for a monocyte was adjusted, because monocytes are larger than nuclei. (5-9µm for nuclei, more than 10µm for monocytes). The ratio of monocytes to endothelial cells was subsequently calculated and used as standardized expression of monocyte adhesion to the endothelial microvessel.

Immunohistochemistry

Endothelial microvessels were fixed using 3.7% formaldehyde (Sigma-Aldrich 252549) in HBSS (Sigma-Aldrich H6648) for 20 minutes, washed twice with HBSS for five minutes, and permeabilized with 0.3% Triton X-100 (Sigma-Aldrich T8787) in HBSS for 10 minutes. After washing with 4% FBS in HBSS for five minutes, the HCAECs were incubated with a blocking buffer (2% FBS, 2% bovine serum albumin [Sigma-Aldrich A2153]) and 0.1% Tween 20 (Sigma-Aldrich P9416) in HBSS for 45 minutes. After blocking, cells were incubated for 90 minutes with a primary antibody solution, washed three times with 4% FBS in HBSS, and incubated with a secondary antibody and nuclear staining for 30 minutes. All steps were performed at room temperature. The primary antibodies used were mouse anti-human antibodies for ICAM-1 at 5 µg/mL (1:100, Bio-Techne BBA3; Minneapolis, MN, USA) and CD31 at 10 µg/mL (Dako M0823) and rabbit anti-human antibodies for VE-cadherin at 1 µg/mL (Abcam, Ab33168; Cambridge, UK). The secondary antibodies were goat anti-mouse Alexa Fluor 488 at 8 µg/mL (Invitrogen A11001; Carlsbad, CA, USA) and goat anti-rabbit Alexa Fluor 488 at 8 µg/mL (Invitrogen A11008). For nuclear staining, Hoechst 33342 (Thermo Fisher Scientific H3570) at 5 µg/mL was used.

Images were captured using an ImageXpress XLS-C HCI system. For quantification of the immunofluorescent staining, z-series were captured, and the sum projection was saved. Quantification was performed by calculating the mean intensity of the captured image in Fiji divided by the number of nuclei observed.

Transcriptomic analysis of endothelial microvessels stimulated by TNFα

Microvessel lysis

HCAEC microvessels were lysed by applying 40 µL of lysis buffer (consisting of 1% beta-mercaptoethanol [Sigma-Aldrich M6250] in Buffer RLT [QIAGEN 79216; Hilden, Germany]) to the perfusion inlet and 10 µL lysis buffer to the perfusion outlet, creating a flow through the microfluidic channel. After 30 seconds, the lysate was collected in a polymerase chain reaction clean tube (VWR 211-2120; Radnor, PA, USA). Seven microfluidic chips were pooled into a total volume of 240 µL lysis buffer and stored at −80°C for transcriptomics analysis.

RNA extraction and profiling

Samples from pooled HCAEC microvessel lysates from four independent experiments were randomized, and RNA was extracted on a QIAcube robot (batch of 12 samples) using the RNeasy Micro Kit (QIAGEN 74004) and then stored at −80°C. Purified RNA was quantified using a Nanodrop ND-1000 (Thermo Fisher Scientific). The RNA integrity number was determined using an Agilent 2100 Bioanalyzer with the Agilent RNA 6000 Pico Kit (Agilent Technologies 5067-1513; Santa Clara, CA, USA); RNA integrity number values ranged from 6.8 to 10 (mean: 9.58). RNA was processed in a 96-chip plate (same batch) and required 50 ng of total RNA on a fully automated Biomek FXp robot (Beckman Coulter, Brea, CA, USA) with the NuGEN Ovation RNA amplification system V2 protocol (3100-A01; San Carlos, CA, USA). Single-primer isothermal amplification was followed by fragmentation and biotinylation of the cDNA. Hybridization was performed overnight (16 hours)

at 60 rpm in a 45°C GeneChip® Hybridization Oven 645 (Affymetrix, Santa Clara, CA, USA) on a GeneChip Human Genome U133 Plus 2.0 Array (Affymetrix), which measures the expression of more than 47,000 transcripts. The sequences from which these probe sets were derived were selected from GenBank™, dbEST, and RefSeq sequence databases. Arrays were washed and stained on a GeneChip® Fluidics Station FS450 DX (Affymetrix) using the Affymetrix GeneChip™ Command Console Software (AGCC software version 3.2, protocol FS450_0004).

Transcriptomic data processing and pairwise comparisons

Summarization and normalization of probes in the raw data (CEL files with access ID E-MTAB-7555 are available in the ArrayExpress public repository database) were performed using Entrez-based probe annotation HGU133Plus2_Hs_ENTREZG cdf version 16.0.0[26] and frozen robust microarray analysis (fRMA),[27] respectively. The normalization vector HGU133Plus2_fRMAvecs version 1.3.0 was used with the R package fRMA version 1.18.0. Quality controls, including log intensities, normalized unscaled standard error, relative log expression, median absolute value of relative log expression, and pseudo-images and raw image plots, were performed with the affyPLM package version 1.42.0 (Bioconductor suite).[28] After quality control, pairwise comparisons at the gene level, called systems response profiles (SRP), were computed by comparing each concentration treatment with its respective vehicle control (VC) using the Bioconductor Limma R package version 3.22.1.[29] No gene was filtered out at any step of the computational analysis. Genes with a false discovery rate (FDR) below 0.05 (p-value adjustment using the Benjamini and Hochberg method) were considered differentially expressed.[30] For biological interpretation, SRPs including all genes (18,604) were analyzed using p-value threshold-free computational approaches (gene set enrichment analysis and network perturbation amplitude (NPA) analyses described below). Most R packages used to conduct the data analysis were included in Bioconductor version 3.0. The R version used was 3.1.2.

NPA analysis

Using transcriptomic data and biological cause-and-effect network models, we applied a computational approach that quantifies a response to a stimulus to analyze network perturbation[31] in HCAEC microvessels. A network is an assembly of directed and signed causal relationships between molecular biological entities that collectively model a specific biological process in a defined context (e.g., lung or vascular). The causal relationships have been curated from the scientific literature and encoded in Biological Expression Language syntax. The network is composed of functional (backbone) and transcript (gene expression) layers. The backbone node-level and network-level perturbation amplitudes can be calculated by considering the measured gene expression changes and the network topology using a backward-causal reasoning algorithm. Three statistics are computed to assess the significance of an NPA score with respect to biological variation (confidence interval) and its specificity to the given two-layer network structure (O and K statistics). A collection of biological networks representative of the main processes of cell fate, inflammation, repair, stress, and proliferation has been published and is accessible at http://causalbionet.com.[32,33] We report here the NPA scores for the vascular inflammatory processes/endothelial cell-monocyte interaction network model in the scope of this manuscript.

Principal component (PC) analysis (PCA) and pathway enrichment analysis

Gene set enrichment analysis was conducted to identify biological pathways/processes associated with genes that drive the discrimination of concentration and exposure time of HCAEC microvessels to TNFα. After performing PCA of the gene expression fold-change (FC) matrix, genes were ranked by their contribution to PCs that explained the maximum of variance. Gene set enrichment analysis was performed using the MSigDB C2-CP gene set collection to identify enriched gene sets representative of biological canonical pathways/processes.[34] Gene resampling (Q1) was performed to generate the null hypothesis distribution and compute the significance associated with each gene set.[35]

Preparation of THS 2.2- and 3R4F-conditioned media from MM6 cells

Generation of fresh aqueous extracts from THS 2.2 aerosol or 3R4F smoke

Mainstream smoke from the 3R4F reference cigarette (Kentucky Tobacco Research Center, University of Kentucky, Lexington, KY, USA) was generated on a 20-port rotary Borgwaldt smoking machine (Hamburg, Germany) according to the Health Canada Intense protocol: 55 mL puff volume, 30-second puff interval, with all ventilation holes blocked.[36] The smoke generated from six reference cigarettes was bubbled through 36 mL of ice-cold RPMI 1640 culture medium to trap the water-soluble fraction, resulting in a stock solution concentration of approximately 1.8 puffs/mL, corresponding to about 10.7 puffs per cigarette, on average. Mainstream aerosol from the candidate MRTP THS 2.2, developed by Philip Morris International, was produced using a pre-defined puff count of 12 puffs per stick on a 30-port rotary aerosol generator (type SM 2000 P1), according to the Health Canada protocol. The aerosol was bubbled into ice-cold RPMI 1640 culture medium to trap the water-soluble fraction (10 HeatSticks/40 mL; stock solution concentration: three puffs/mL). Previous analysis of aqueous extracts showed that the concentrations of carbonyls decreased significantly in THS 2.2 aqueous extract compared with concentrations in 3R4F aqueous extract, while nicotine remained at comparable concentrations in both extracts.[17,18]

Exposure of MM6 cells to fresh THS 2.2 or 3R4F aqueous extracts to generate conditioned media

An MM6 cell suspension was adjusted to 2×10^6 cells/mL in RPMI 1640 medium supplemented with 10% FBS, and 0.5 mL/well was seeded in a 24-well plate. MM6 cells were exposed to various concentrations of 3R4F/THS 2.2 aqueous extract or culture medium/10% FBS (VC) for two hours. Culture supernatants, namely conditioned media, were collected and stored at −80 °C for the adhesion assay.

Treatment of endothelial microvessels with TNFα or 3R4F/THS 2.2-conditioned medium prior to adhesion assay and marker staining

On the fourth day after seeding, endothelial microvessels were treated with TNFα (ImmunoTools 11343015; Friesoythe, Germany) as a positive control for inflammation, with L-buthionine-sulfoximine (25 µM, Sigma-Aldrich B2515) or ethacrynic acid (25 µM, Sigma-Aldrich E4754) as positive controls for GSH depletion, or with 3R4F- or THS 2.2-conditioned medium for four or 16 hours. The four hours time point was used for comparison with previous results obtained in a static 2D endothelial cell model.[18,37] Adhesion proteins, such as SELE, are already maximally expressed after four hours in endothelial cells, and their expression may be transient and decrease at later time points, while the expression of other adhesion proteins, such as vascular cellular adhesion molecule 1, is maintained or triggered at later time points (i.e., 16 hours).[38] At the four hours time point, primary effects of a stimulus can be investigated, while at later time points, secondary activation occurs via feedback loops. At the end of the treatment, endothelial microvessels were either fixed for specific marker immunohistochemistry staining, lysed for transcriptomic analysis (only for TNFα treatment), or directly nuclear stained and used for the adhesion assay under flow.

Measurement of GSH content

Endothelial microvessels were incubated with MV2 medium containing 0.125 mg/mL monochlorobimane (Sigma-Aldrich 69899) and 5 µM DRAQ5 (Abcam ab108710) for 30 minutes at 37 °C and 5% CO2 on a rocking platform (eight-minute intervals at a 7° angle). After washing with HBSS, the z-series were captured on an ImageXpress XLS-C HCI system. Quantification of the intensity of the fluorescent signal was performed in Fiji. Sum projections were acquired from the z-series, and the mean intensity was calculated after subtracting the background. Subsequently, the intensity per counted nucleus was calculated.

Water-soluble tetrazolium salt (WST-8) viability assay

Medium in endothelial microvessels was replaced with MV2 medium containing Cell Counting Kit-8 solution (1:11 dilution, Sigma-Aldrich 96992) and incubated at 37 °C and 5% CO2 for 30 minutes on a rocking platform (eight-minute intervals at a 7° angle). After incubation, the absorbance was measured at 450 nm on a plate reader (Multiskan FC, Thermo Fisher Scientific). The measurements of the gel inlet, perfusion inlet and outlet, and observation window were adjusted for volume differences and combined after background subtraction of the positive cell free control. Analysis was performed in Microsoft Excel (Redmond, WA, USA). Data was normalized to the negative control (MV2 →MV2 0 pg/mL TNFα for the "starvation experiment" and the conditioned medium vehicle control (corresponding to supernatant of MM6 cells exposed to 0 puffs/ml smoke/aerosol aqueous extract) for the "conditioned medium exposure experiment".

Statistical analysis

Statistical analysis was conducted in GraphPad Prism (La Jolla, CA, USA). The mean values for all within-OrganoPlate® chip replicates were calculated and normalized to the control (ratio value/control). Statistical analysis was performed with a one- or two-way analysis of variance (ANOVA) followed by post-hoc Dunnett's pairwise comparisons. The number of replicates for chips within an OrganoPlate® (n) and independent experiments (N) is indicated in the figure legends for each experiment.

Results

Development and optimization of conditions for the formation of endothelial microvessels

Endothelial microvessels were cultured in the two-lane 400-µm OrganoPlate® (Figure 2A). HCAEC vessel formation was optimized for seeding density (Figure 2B), ECM (Figure 2C), and medium composition (Figure 2D). Rapid vessel formation and vessel stability for at least eight days without ingrowth of HCAECs into the ECM were achieved with a seeding density of 106 cells/mL together with collagen I 4 mg/mL ECM cultured in MV2 medium. All further experiments were conducted using this optimized seeding protocol. To show stable vessel formation and endothelial marker expression, endothelial microvessels were fixed at different time points; 3D reconstructions show the reproducible formation of a complete vessel after two days. The vessel remained stable with regards to the expression of CD31 (PECAM-1), VE-cadherin at the junctions (Figure 2E) and low expression of the apoptosis markers caspase 3/7 (supplementary Figure 1) for at least eight days (Figure 2E).

Barrier integrity increases in the course of endothelial microvessel formation and remains stable up to eight days

To assess barrier formation in the HCAEC microvessels, a barrier integrity assay was performed (Figure 3A). Briefly, a fluorescent reporter molecule was perfused through the lumen of the vessel (perfusion channel) and followed over time to assess the diffusion of the reporter into the gel channel. The fluorescence intensity of the medium and gel channel was measured to calculate the apparent permeability coefficient. The barrier integrity assay was performed with three sizes of dextran molecules (4.4, 20 and 155 kDa). Representative images of microvessels at different time points are shown in Figure 3B. Figure 3C shows barrier formation over time. One day after introducing the HCAECs into the microfluidic channels, the diffusion of both 4.4-kDa and 20-kDa dextran through the barrier began

to decrease compared with diffusion in controls without cells, indicative of the formation of an endothelial cell barrier that remained stable for up to eight days.

Establishment of a monocyte-endothelial microvessel adhesion model under flow

To test the endothelial microvessel model for monocyte attachment, fluorescently labeled MM6 monocytes were introduced into the endothelial microvessels after vessel stimulation with increasing concentrations of TNFα for four or 16 hours under flow. After 15 minutes of incubation under perfusion flow, non-attached monocytes were washed away, and the adherent monocytes were quantified. Representative images are shown in Figure 4A. Quantification shows a significant concentration-dependent upregulation of monocyte attachment after stimulation for four and 16 hours for all tested concentrations of TNFα compared with attachment in the VC (Figure 4B). At the four hours time point, the FC of adherent monocytes reached a plateau at concentrations of 50–100 pg/mL (Figure 4B). At the 16 hours time point, the FC of adherent monocytes tended to decrease at the lowest tested concentrations (100 and 500 pg/mL) of TNFα, but was maintained at higher concentrations (500 and 1,000 pg/mL) and increased at the highest concentration (10,000 pg/mL), compared with the FCs at the four hours time point (Figure 4B). In parallel to monocyte adhesion, ICAM1, an adhesion molecule expressed by endothelial cells to which monocytes bind (Figure 4C), was quantified in endothelial microvessels. Stimulation of the endothelial microvessels with TNFα significantly upregulated ICAM1 protein levels in HCAECs in a concentration-dependent manner compared with levels in the VC. Representative images are shown in Figure 4D, and quantification of the immunofluorescent images is shown in Figure 4E. Longer stimulation with high concentrations of TNFα (more than 500 pg/mL) resulted in higher ICAM1 levels. The profiles of concentration-dependent ICAM1 protein abundance FCs observed at four and 16 hours correlated positively with those of monocyte-endothelial microvessel adhesion at the corresponding time points (Figure 4B and E).

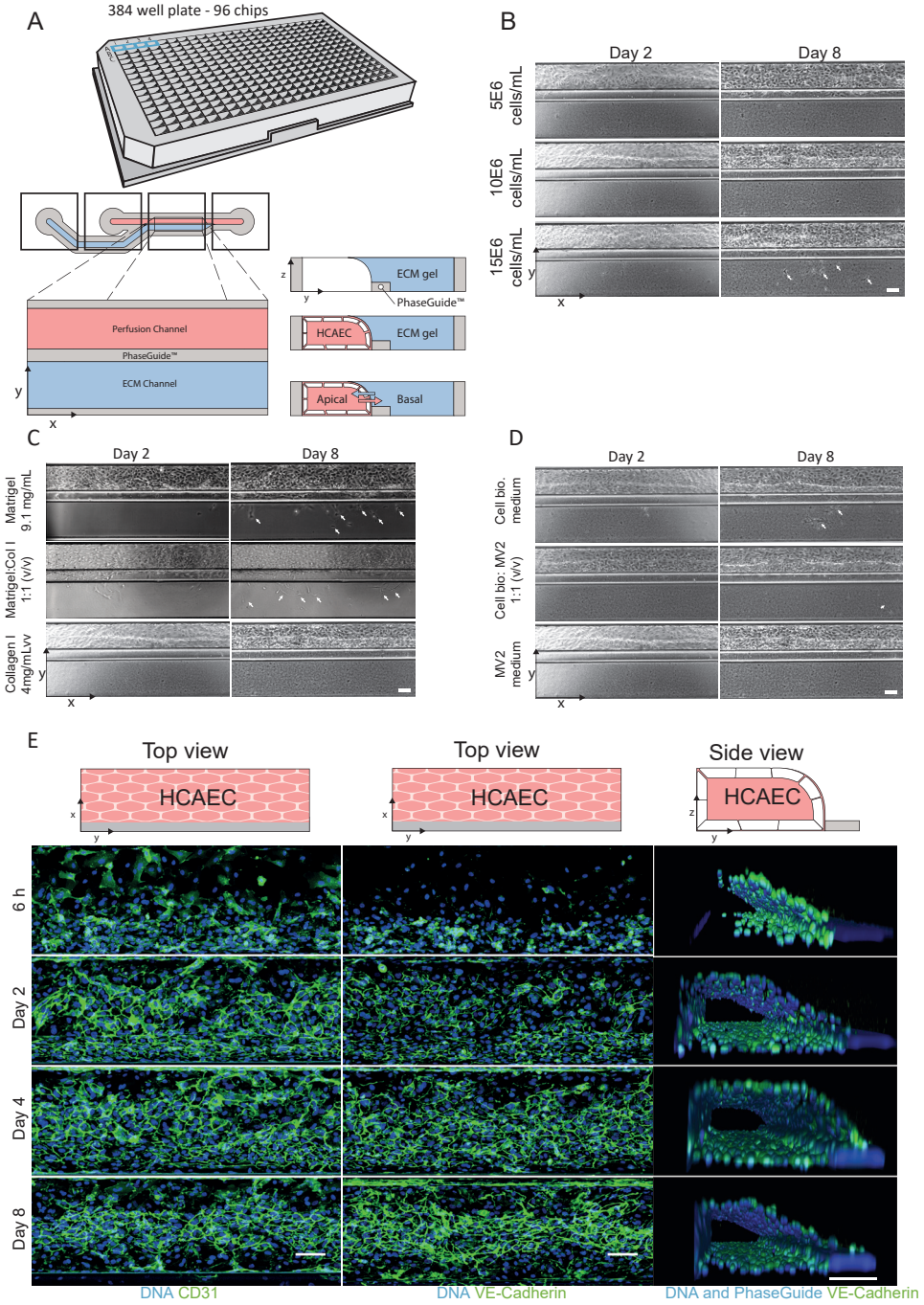

Figure 2. 3D endothelial microvessel culture formation and optimization. (A) Schematic overview of the OrganoPlate®. A gel channel (blue) holds an ECM in place

through the PhaseGuide's pressure barrier function. Endothelial cells are seeded in the adjacent medium perfusion channel (red). Upon the addition of perfusion flow, a tubular structure is formed in the medium channel. (B–D) 3D culture optimization of primary human coronary artery endothelial cells on the OrganoPlate® platform. The platform was optimized for cell seeding density **(B)**, ECM composition **(C)**, and medium composition **(D)** to select the optimal cell culture conditions. Phase contrast pictures were taken two and eight days after seeding, and the optimal conditions (barrier formation and no invasion of the ECM) were selected for subsequent experiments. White arrows indicate invasion of cells into the ECM on day eight. **(E)** Maximum projection and 3D reconstruction of a confocal z-stack of the cells in the tissue chips using the optimized seeding conditions (106 cells/mL, collagen I at 4 mg/mL ECM, and MV2 medium). HCAEC microvessels were fixed six hours and two, four and eight days after seeding and stained for DNA and the adherens-junction markers CD-31 and VE-cadherin. The maximum projections and 3D reconstruction show barrier formation and stable tubular morphology with a lumen two to eight days after seeding. Scale bar = 100 µm. Abbreviations: h, hours.

Transcriptomic analyses of HCAEC microvessels stimulated by TNFα for four and 16 hours

Transcriptome analysis of HCAEC microvessels enabled the investigation of molecular changes at the mRNA transcript level following treatment with TNFα for four and 16 hours. SRPs (or contrasts) were computed by comparing each TNFα treatment group with its respective VC using linear modeling. A PCA plot of the FC matrix visualized the sources of variation in gene expression data. Scores (treatment groups) and loadings (genes contributing to the discrimination of treatment groups) were visualized on a biplot for PC1-PC2 sub-space, both PCs explaining 73.1% of the total variance (Figure 5A and B), and revealed time and concentration effects, with a clear separation of SRPs mostly along PC1 and PC2, respectively. Top genes with the largest positive and negative loading values for PC1 and PC2 (Figure 5B) showed specific FC expression patterns across concentrations and time points (Figure 5C). For biological interpretation, all genes were ranked by their contribution to PC1 or PC2, and gene set enrichment analysis was performed using the MSigDB C2-CP gene set collection representative of canonical pathways/biological processes. Gene sets grouped by their positive and negative enrichment scores were scattered in the four quadrants of the PCA biplot. The top five significant (FDR < 0.05 for at least one PC) gene sets for each quadrant are highlighted in Figure 5D. The results show an enrichment of gene sets reflective

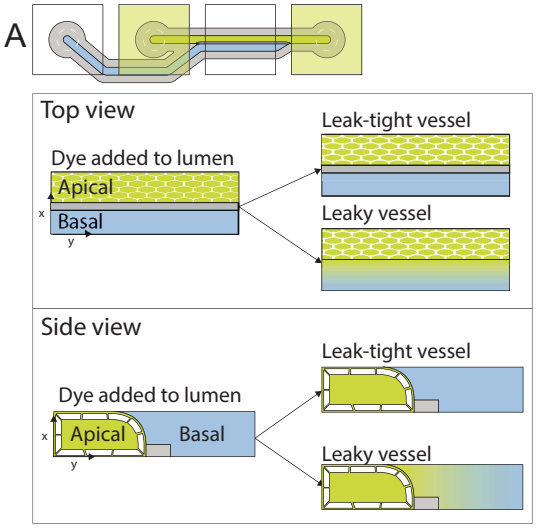
A
Top view
Dye added to lumen
Apical
Basal
x
y
Leak-tight vessel
Leaky vessel
Side view
Dye added to lumen
Apical
Basal
x
y
Leak-tight vessel
Leaky vessel

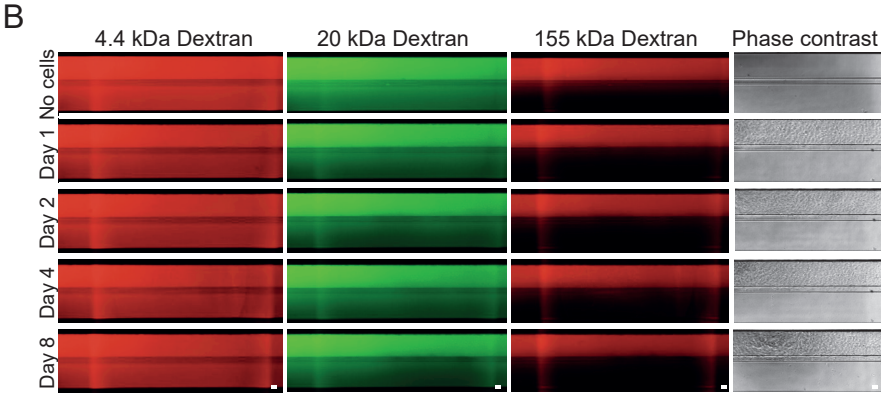
B
4.4 kDa Dextran
20 kDa Dextran
155 kDa Dextran
Phase contrast
No cells
Day 1
Day 2
Day 4
Day 8

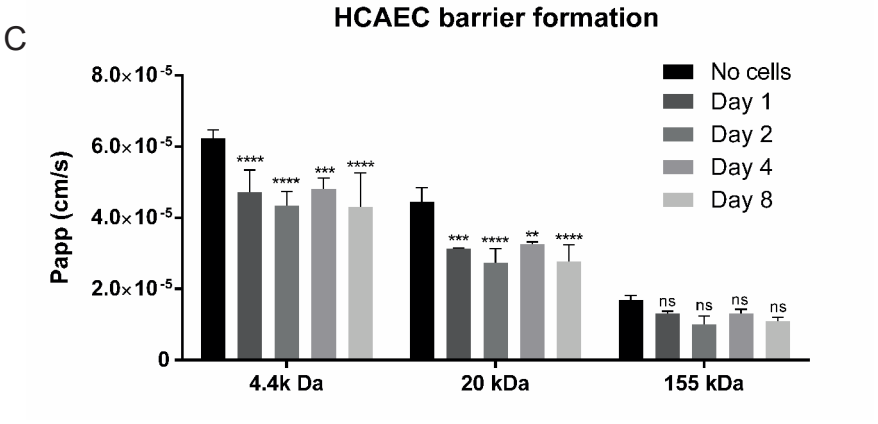
C
HCAEC barrier formation
Papp (cm/s)
8.0×10-5
6.0×10-5
4.0×10-5
2.0×10-5
0
No cells
Day 1
Day 2
Day 4
Day 8
4.4k Da
20 kDa
155 kDa

Figure 3. Barrier formation in HCAECs. (A) Principle of the barrier integrity assay in the OrganoPlate®. A fluorescent dye is added to the lumen of the vessel, and the integrity of the barrier is quantified by measuring the intensity of fluorescent dye diffusing into the adjacent gel channel. **(B)** Fluorescent images show HCAEC barriers for both 4.4 kDa FITC-dextran, 20 kDa FITC-dextran and 155 TRITC-dextran one to eight days after seeding. The fluorescent images were taken 14 minutes after addition of the dye. Scale bar = 100 µm **(C)** Papp index of the HCAEC barrier over time. Plot bars represent the mean + standard deviation (N = 3, n ≥ 7). ns = not significant, **p < 0.01, ***p < 0.001, ****p < 0.0001 (two-way ANOVA).

of inflammation (e.g., KEGG_CYTOKINE_CYTOKINE_RECEPTOR_INTERACTION, PID_CD40_PATHWAY), protein post-translational modification (e.g., REACTOME_BIOSYNTHESIS_OF_THE_N_GLYCAN_PRECURSOR_DOLICHOL_LIPID_LINKED_OLIGOSACCHARIDE_LLO_AND_TRANSFER_TO_A_NASCENT_PROTEIN), cell cycle/DNA replication (e.g., REACTOME_E2F_MEDIATED_REGULATION_OF_DNA_REPLICATION), and mitosis (e.g., PID_AURORA_B_PATHWAY, REACTOME_MITOTIC_PROMETAPHASE) pointed in the direction of the Q1, Q2, Q3, and Q4 quadrants, respectively (Figure 5D and Supplementary Table 1). The selection of differentially expressed genes (DEG) (FDR < 0.05) revealed a TNFα concentration-dependent increase of significantly upregulated and downregulated genes with a lower effect at 16 hours than at four hours (Figure 5E). To verify consistency between molecular changes and functional readouts, we conducted a network perturbation analysis, leveraging each SRP and a causal network model representative of monocyte-endothelial cell adhesion mechanisms. Figure 5F shows a TNFα concentration-dependent increase in the NPA similar to the readout observed with the MM6 cell-HCAEC microvessel adhesion assay (Figure 4B). Interestingly, the nodes with the larger significant amplitude scores across SRPs were "p(HGNC:ICAM1)" and "path(SDIS:monocyte_adherence)," corresponding to predicted activation of the protein ICAM1 and the adhesion of monocytes to the endothelium, respectively (Supplementary Table 2). This result was supported by an increased expression of mRNA transcripts coding for adhesion molecules as measured by Affymetrix microarray (Supplementary Figure 2). We then compared the response to TNFα in our 3D model and a 2D model to assess whether a similar biology was perturbed. For this purpose, we retrieved an SRP from a previous study, corresponding to the

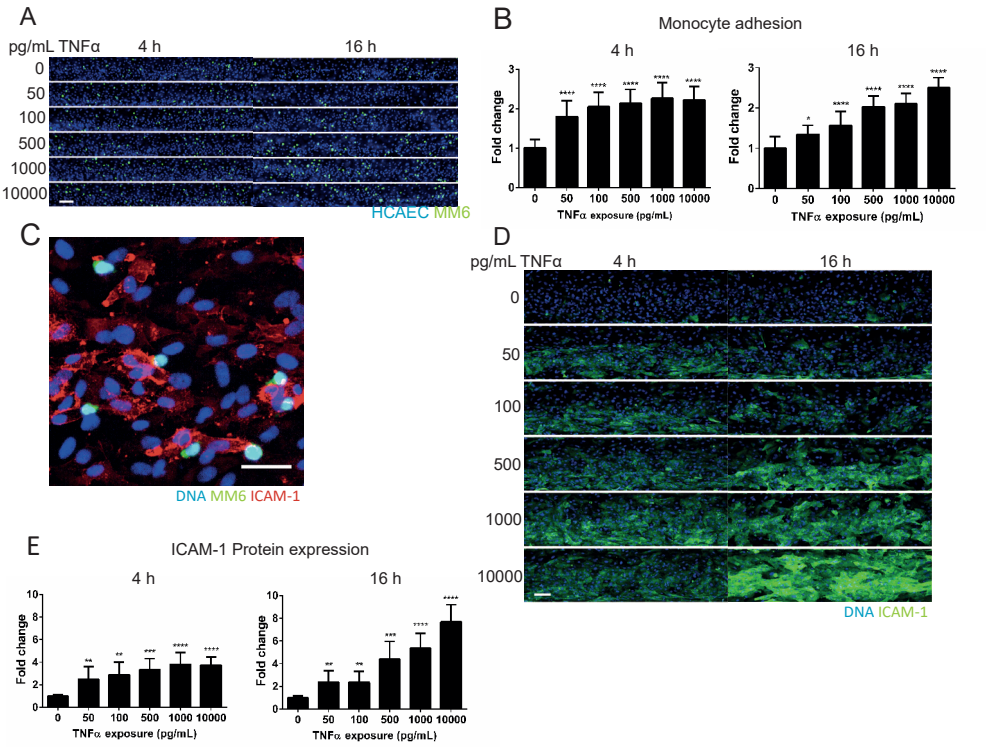

Figure 4. Establishment of a monocyte-endothelial microvessel adhesion model under flow. (A) Monocyte adhesion after four or 16 hours of TNFα exposure. MM6 monocytes labeled with live stain calcein AM were added under flow to the endothelial microvessel (pre-stained with the nuclear dye Hoechst 33342) for 15 minutes. After washing, fluorescent images were captured (scale bar = 50 µm) and the number of attached monocytes (green) per nucleus (blue) was calculated. **(B)** The plot shows the mean increase compared to the VC + standard deviation. *p < 0.05, ****p < 0.0001 (one-way ANOVA followed by post-hoc Dunnett's pairwise comparisons) compared with VC. N = 2–3, n = 6. **(C)** High magnification of monocyte-endothelial attachment (scale bar = 50 µm). (D and E) Images and quantification of the protein adhesion marker ICAM1 in the endothelial microvessel after four or 16 hours of exposure to TNFα. The intensity of the immunofluorescent ICAM1 staining was measured per nucleus of HCAECs. N = 3, n = 3. The plots show the fold change relative to the VC corresponding to the condition with no TNFα (mean + standard deviation). **p < 0.01, ***p < 0.001, ****p < 0.0001 (one-way ANOVA followed by post-hoc Dunnett's pairwise comparisons). Abbreviations: h, hours.

conditions of 2D monolayer HCAECs treated with 10 ng/mL of TNFα for four hours and the respective VC.[17] Leveraging the same conditions using our 3D model, a comparison of gene expression FCs and pathway-based gene set enrichment scores revealed a high consistency between the 3D and 2D models (Figure 5G and H; Supplementary Table 3). The correlation increased notably when selecting

significant genes (FDR < 0.05) and gene sets (FDR < 0.10), highlighted as red dots on the scatter plots (Figure 5G and H). A subset of gene sets was inversely correlated with the enrichment scores, which were not significant (Figure 5H).

Model application for product toxicological assessment: use case with a heat-not-burn tobacco product compared with a reference product

As an application of the established monocyte-endothelial microvessel adhesion model, we assessed the impact of a candidate MRTP, THS 2.2, compared with that of the 3R4F reference cigarette on the adhesion of monocytic cells to endothelial microvessels, a key step in the initiation of atherogenesis. In a previously established 2D and static adhesion assay, HCAECs were exposed to conditioned medium generated from human monocytic MM6 cells treated with various concentrations of aqueous extract of 3R4F smoke or THS 2.2 aerosol.[18] We used the same type of endothelial microvessel exposure.

Reduced effect of THS 2.2 aqueous extract compared with that of 3R4F aqueous extract on TNFα release by MM6 cells

Cigarette smoke-derived chemicals that are water-soluble can interfere with serum proteins present in the culture medium, potentially reducing the effect of the smoke/aerosol aqueous extract.[39] To limit this, conditioned medium is, in principle, generated using starvation medium by reducing the percentage of FBS from 10% to 0.5%. The supplementary Figure 3 shows that the adaptation of HCAEC microvessels to medium with low serum content (0.5% FBS) affected HCAEC viability/proliferation and number of cells, as measured by WST-8 enzymatic activity (panels A – D) and nuclei count (panels E – H), respectively, after four and 16 hours. Therefore, we decided to generate conditioned medium by maintaining the serum content at 10% FBS and measure the levels of TNFα

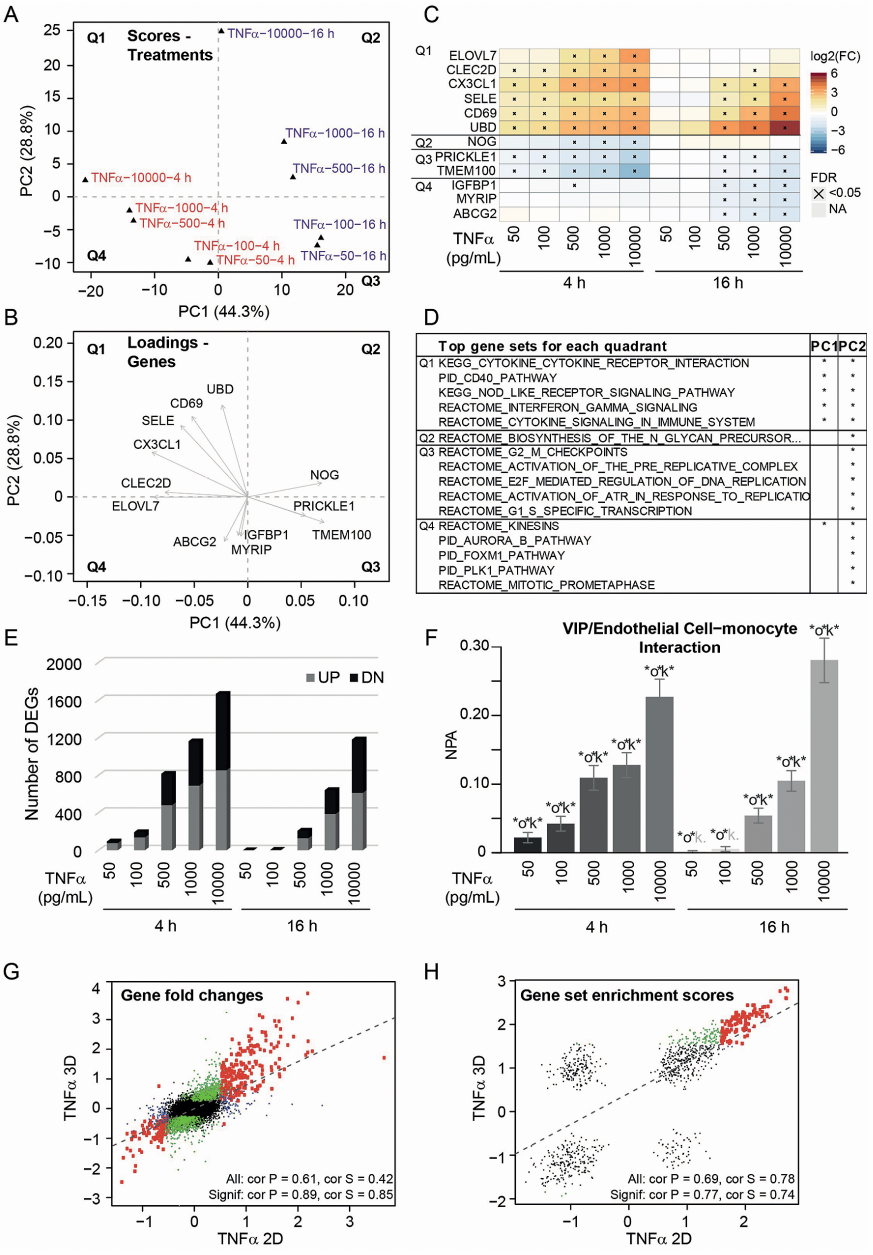

Figure 5. Transcriptomic analysis of HCAEC microvessels at day 4 treated with various concentrations of TNFα for 4 and 16 hours. PC1-PC2 sub-space scatterplots of **(A)** treatment group scores and **(B)** gene loadings following principal component analysis of FC gene expression matrix. **(C)** Heatmap of expression FCs (in log2 scale) of the top six genes per principal component contributing the most to the separation of

treatment groups. **(D)** Top gene sets associated with genes pointed in the direction of the four quadrants of the PC1-PC2 sub-space scatterplot. Gene sets were ranked by their average FDRs associated with PC1 and PC2 enrichment scores, and the top five gene sets (if more than five gene sets appeared on the list) were extracted and displayed. The full list of significant gene sets is provided in Supplementary Table 1. **(E)** Barplot of DEGs (FDR < 0.05) for all systems response profiles. **(F)** Barplot of NPA scores for microvessel systems response profiles graphed using the vascular inflammatory processes/endothelial cell-monocyte interaction network model. Scores are shown with their confidence intervals accounting for experimental variation. A network is considered perturbed if, in addition to the significance of the NPA score with respect to the experimental variation, the two companion statistics (O and K) derived to inform the specificity of the NPA score with respect to the biology described in the network are significant. *O and K statistic p-values below 0.05 and NPA significance with respect to the experimental variation. p-values between 0.05 and 0.1 for "O" and "K" (in grey). **(G)** Scatterplot of gene expression FCs in log2 2D vs. 3D models (TNFα, 10 ng/mL, four hours exposure). **(H)** Scatterplot of gene set enrichment scores for 2D and 3D models (TNFα, 10 ng/mL, four hours exposure). For panels G and H, data points highlighted in red, green, and blue correspond to genes or gene sets that are significant in both 3D and 2D models, in the 3D model only, and in the 2D model only, respectively. The dotted line corresponds to the regression line when considering all genes or gene sets for the linear model. All Spearman and Pearson correlation coefficients were computed using all genes/gene sets; significant genes/gene sets were highly significant ($p < 0.0001$). The full list of significant gene sets is provided in Supplementary Table 3. For the 3D model, N = 4 independent experiments, n = 7 microvessels pooled in one lysate. Abbreviations: cor P, Pearson's correlation coefficient; cor S, Spearman's correlation coefficient; DN, downregulated; Signif, significant; UP, upregulated; h, hours.

released by monocytic cells in conditioned medium as a quality check showing similar results to previous work done in low serum content conditions.[17,18]

We previously showed that TNFα, a surrogate inflammatory marker, was released by MM6 cells in the starvation medium following a two-hour treatment with 3R4F aqueous extract.[37] Therefore, the concentration of TNFα was determined in 3R4F- and THS 2.2-conditioned media containing 10% FBS (Figure 6B). The results show a concentration-dependent augmentation of TNFα reaching a maximum at 0.05 puffs/mL of 3R4F aqueous extract and then decreasing at higher concentrations (0.1 and 0.25 puffs/mL). At the concentration of 0.05 puffs/mL of 3R4F aqueous extract at which a TNFα peak was measured, no significant TNFα release was observed for the THS 2.2 aqueous extract exposure. It was necessary to enhance the concentration of THS 2.2 aqueous extract (0.7 puffs/mL) by a factor of approximately 14 to measure TNFα levels in the conditioned medium that were similar to those obtained with the 3R4F aqueous extract exposure (Figure 6B).

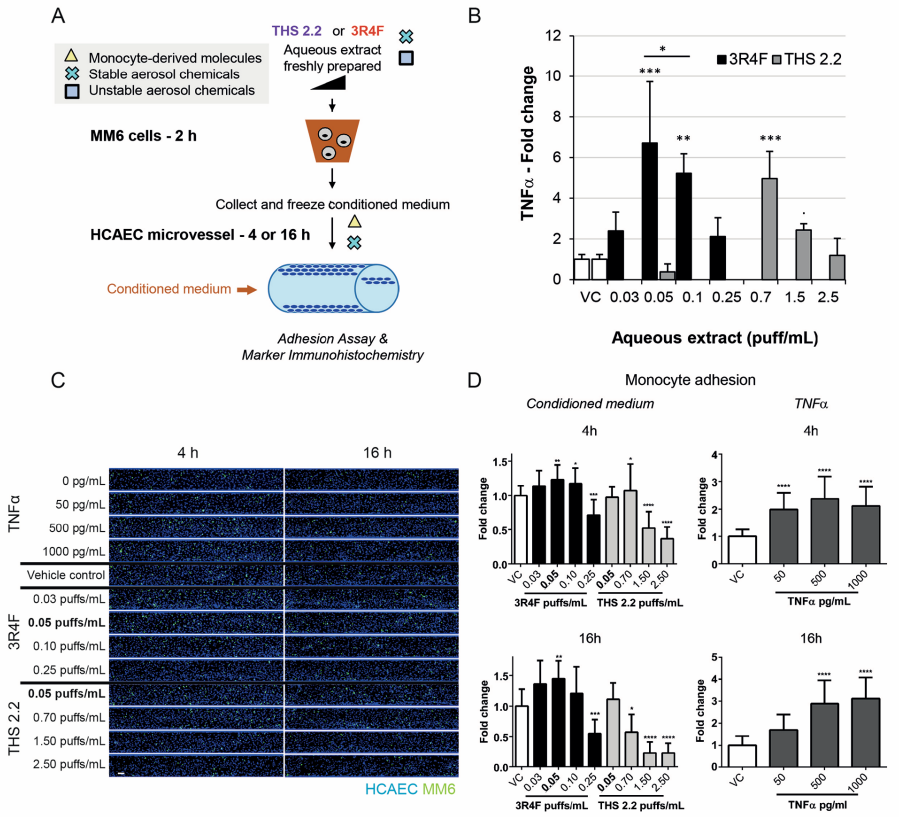

Figure 6. Vasculature-on-a-chip application for assessment of THS 2.2: monocyte-to-endothelial microvessel adhesion under flow. (A) Scheme of experimental design. **(B)** TNFα release in conditioned medium following a two-hour exposure of MM6 cells to freshly generated aqueous extract from 3R4F cigarette smoke or THS 2.2 aerosol. N = 4, n = 2. **(C)** Representative images of monocyte attachment to 4 day-HCAEC microvessels after exposure to TNFα or conditioned medium for four and 16 hours. **(D)** Quantification of monocyte adhesion after conditioned medium exposure. MM6 attachment to the endothelial microvessels was measured four and 16 hours after addition of the conditioned medium. Attachment was quantified as the number of MM6 cells attached per 100 HCAECs and normalized for the VC corresponding to conditioned medium without 3R4F smoke/THS2.2 aerosol aqueous extracts. N = 4, n = 4–6. .p<0.1, *p < 0.05, **p < 0.01, ***p < 0.001, ****p < 0.0001 compared with attachment in VC (one-way ANOVA followed by post-hoc Dunnett's pairwise comparisons). Abbreviations: h, hours.

Reduced effect of THS 2.2-conditioned medium compared with that of 3R4F-conditioned medium on MM6 cell adhesion to HCAEC microvessels

After exposure of HCAEC microvessels to 3R4F-conditioned medium for four and 16 hours, the adhesion of MM6 cells to the lumen of microvessels increased significantly and peaked at a concentration of 0.05 puffs/mL of 3R4F aqueous extract (Figure 6C and D). At this concentration, THS 2.2-conditioned medium did not significantly promote the adhesion of MM6 cells to HCAEC microvessels (Figure 6C and D). The concentration of THS 2.2 aqueous extract (0.7 puffs/mL) in conditioned medium had to be enhanced by a factor of approximately 14 to yield similar adhesion (Figure 6D). At 16 hours, no significant increase in adhesion was measured at any concentration of THS 2.2 aqueous extract in conditioned medium, and adhesion actually decreased significantly at the highest concentrations of THS 2.2 aqueous extract (1.5 and 2.5 puffs/mL) (Figure 6D). In parallel, various concentrations of TNFα were included as positive controls and yielded similar results (Figure 6C and D) to those observed (Figure 4) in establishing the adhesion assay with HCAEC microvessels.

Reduced effect of THS 2.2-conditioned medium compared with that of 3R4F-conditioned medium on ICAM1 protein abundance and GSH content in HCAEC microvessels

ICAM1 protein was stained and quantified in HCAEC microvessels, and patterns of ICAM1 protein abundance changes similar to those observed for MM6-HCAEC microvessel adhesion were measured after four or 16 hours of exposure to conditioned medium (Figure 7A and B). Exposure to conditioned medium did not affect the viability of the microvessel cultures, except at the highest concentration (2.5 puffs/mL) of THS 2.2 aqueous extract (Supplementary Figure 4A). The number of nuclei counted in the vessels was not affected by conditioned medium exposure (Supplementary Figure 4B), indicating low toxicity of the conditioned medium at these incubation time points. In addition to soluble mediators released by MM6 cells, conditioned medium contains chemical constituents derived from cigarette

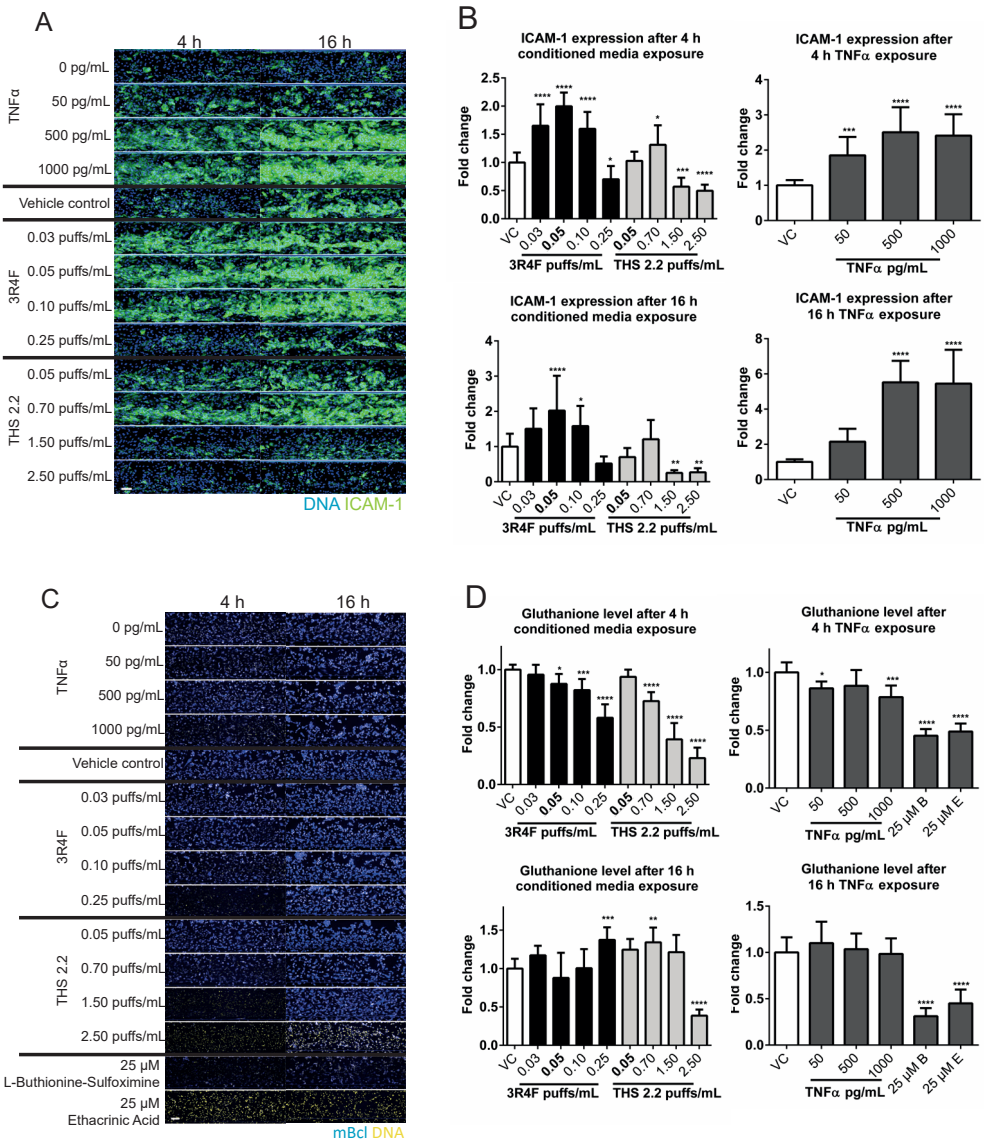

Figure 7. Vasculature-on-a-chip application for assessment of THS 2.2: quantification of key inflammatory and oxidative stress markers. HCAEC microvessels at day 4 were treated with 3R4F- and THS 2.2-conditioned media or with TNFα (50-1,000 pg/mL), L-buthionine-sulfoximine [B, 25 μM] and ethacrynic acid [E, 25 μM] as positive controls for four and 16 hours. **(A)** Representative pictures (sum-projections) and **(B)** quantification barplots of ICAM1 protein in HCAEC microvessels. N=4, n=3. **(C)** Representative pictures (sum-projections) and **(D)** quantification barplots of GSH content in HCAEC microvessels. N=3, n=3. The results for both markers are expressed as the FC intensity (calculated per HCAEC nucleus) between treatment and its VC. Statistics: *=p<0.05, **=p<0.01, ***=p<0.001, ****=p<0.0001 (compared to VC, one-way ANOVA followed by post-hoc

Dunnett's pairwise comparisons). Abbreviations: 3R4F, reference cigarette; THS 2.2, Tobacco Heating System 2.2; h, hours.

smoke. We previously showed that these compounds, which remain stable in conditioned medium, after a freezing/thawing cycle, can trigger oxidative stress in endothelial cells on top of an inflammatory response promoted by MM6-derived soluble mediators.[37] Therefore, we measured GSH levels to assess the magnitude of oxidative stress in HCAEC microvessels (Figure 7C and D). We also exposed HCAEC microvessels to 25 µM of L-buthionine-sulfoximine and 25 µM of ethacrynic acid as positive controls. The exposure resulted in a significant reduction in GSH levels after four and 16 hours (Figure 7C and D). Depletion of GSH, indicating oxidative stress, was observed with increased concentrations of 3R4F or THS 2.2 aqueous extracts in conditioned medium; however, the effect on GSH levels was measured when concentrations of THS 2.2 aqueous extract in the conditioned medium were approximately 14 times higher than concentrations of 3R4F aqueous extract. After a 16-hour exposure, GSH levels returned to levels similar to those of the VC, with the exception of GSH levels in microvessels exposed to the highest concentration (2.5 puffs/mL) of THS 2.2 aqueous extract (Figure 7C and D).

Discussion

In this work, we developed and optimized a 3D vasculature-on-a-chip model using the OrganoPlate® platform to investigate the mechanism of leukocyte adhesion to the lumen of endothelial microvessels, a key step in the initiation of inflammation and vascular disorders, such as atherosclerosis. Moreover, we showed how this 3D endothelial vascular model can be leveraged for real-world applications, such as systems toxicology assessments of products in a research and development framework.

In order to establish our 3D model and grow microvessels, we used primary HCAECs, a cellular model particularly relevant in studying cardiovascular diseases. The tubular shape developed within two days only when endothelial cells, adherent to the ECM, were perfused, indicating that the bidirectional and oscillating flow generated by gravity-driven leveling had a mechanical effect on endothelial cells. In this context, cells intermittently undergo a shear stress estimated to rise up to 1.6 dyne/cm2 when the rocker is tilted.[40] In vivo, similar-sized venules are exposed to shear levels between 1 and 5 dyne/cm2.[41] The endothelial barrier increased after a few hours and was formed after two days, remaining stable for at least eight days. After two days, permeability to 4.4 and 20 kDa dextran reached levels (4.0×10−5 cm/s and 3×10−5 cm/s, respectively) comparable with those found in microvessels grown with human umbilical vein endothelial cells.[8] HCAEC barrier formation was characterized by positive stainings of the VE-cadherin and CD31 proteins, two major endothelial-junction-associated proteins playing a role in the process of blood vessel tube formation (Vestweber, 2008; Yang et al., 1999). The nature of ECM and microenvironments can influence the growth and migratory phenotypes of endothelial cells.[42,43] Therefore, we optimized the choice of ECM and culture conditions (medium and cell density) to obtain homogeneous and reproducible HCAEC tubes devoid of cell protrusion/migration into the ECM, a characteristic of angiogenic behavior.[44]

For functional analysis of the model, we set up an adhesion assay by flowing untreated, fluorescently labeled monocytic cells through the lumen of HCAEC microvessels pre-stimulated with TNFα and quantifying the monocytic cells that remained attached to the endothelium. HCAEC microvessels responded to TNFα by promoting the adhesion of monocytic cells to microvessels in a concentration-dependent manner after four hours, with sustained effects at the highest concentrations (500 and 10,000 pg/mL) after a 16-hour treatment. In parallel, the immunohistochemical quantification of ICAM1 in HCAEC microvessels showed a correlation of the adhesion protein with monocyte-endothelium adhesion promoted by TNFα. The kinetic profile of ICAM1 protein expression was consistent with previous findings.[38]

These observations were also supported by TNFα concentration- and time-dependent gene expression changes, clearly showing increased transcription of inflammatory genes following the activation of the TNFα/nuclear factor-kappa B signaling pathway. Gene sets that were significantly enriched reflected innate immune/inflammatory pathways, such as cytokine/chemokine signaling, TNFα/CD40 signaling, and interferon γ signaling, in addition to cell cycle processes, such as DNA replication and mitosis. Interestingly, an analysis of time course protein-protein interaction networks using transcriptomics and genome-wide datasets accompanied by experimental validation has shown that TNFα can promote G1/S transition in the cell cycle in vascular endothelial cells.[45] This may facilitate the cell cycle activation promoted by vascular endothelial growth factor. The comparison in response to TNFα of 3D and 2D endothelial cell models showed high consistency at the levels of gene expression changes and enriched pathways/processes. However, an accurate quantification of differences between both models would require an experiment comparing 3D and 2D cultures simultaneously, using HCAECs from one donor, which was not the case here, although our study was still robust in showing the biology perturbed by TNFα across independent experiments and donors.

Overall, these results indicate that following TNFα stimulation, HCAEC microvessels in vitro can be activated and bind monocytes under flow. The pattern of adhesion correlated with the expression of adhesion molecules, similarly to previous in vivo and in vitro observations in arterial and microvascular endothelial cells.[46–50]

For a real-case application in systems toxicology, our HCAEC microvessel model was leveraged to assess the impact of aerosol from THS 2.2, a candidate MRTP, compared with the impact of 3R4F smoke in the form of conditioned medium on the process of monocytic cell adhesion to endothelial microvessels. The conditioned medium was generated by collecting the supernatant of MM6 cells exposed to aqueous extracts from 3R4F smoke or THS 2.2 aerosol for two hours. Conditioned medium contains a mixture of soluble mediators released by monocytic cells and chemical-derived compounds from smoke/aerosol, mimicking an in vitro milieu with inflammatory and oxidative properties, such as blood from smokers.[12,37,51] The four-hour exposure of HCAEC microvessels to 3R4F-conditioned medium triggered an inflammatory response that promoted an increase in endothelial adhesion proteins and monocytic cell adhesion to the lumen of the HCAEC microvessels as well as endothelial oxidative stress, observed as depletion of GSH. Although the presence of serum during the exposure of HCAEC microvessels to conditioned medium may potentially reduce the effect of aqueous extracts,[39] these findings are similar to previous ones in HCAECs, also showing that monocyte-released soluble mediators, such as TNFα, are responsible for inducing the inflammatory response,[37,52] while chemical compounds derived from 3R4F smoke induced oxidative stress in HCAECs.[37] At the later time point (16 hours), GSH content was restored, indicating that HCAEC microvessels coped with the oxidative stress, while endothelial inflammation was still observed at some concentrations, suggesting a sustained effect of inflammatory mediators present in 3R4F-conditioned medium and/or possible autocrine feedback loops. At concentrations of 3R4F-conditioned medium at which molecular and functional effects peaked, no significant effect was observed with THS 2.2-conditioned medium. It was necessary to increase the concentration of THS 2.2 aqueous

extract to generate conditioned medium by a factor of approximately 14 to record similar effects to those seen for 3R4F-conditioned medium. These results are in agreement with our previous work in a 2D HCAEC adhesion assay model.[17,18] Overall, this case study of leveraging a 3D vasculature-on-a-chip model for risk assessment in vitro shows the potential of water-soluble aerosol extract from THS 2.2 to exert a reduced impact on mechanisms that lead to the development of atherosclerosis in a pathological context, compared with extracts from cigarettes. It should be noted, however, that these findings are specific to an atherosclerosis-related context, and effects may differ in other disease models or physiological systems, underscoring the need for broader investigation before general conclusions can be drawn.

The microvessel model was used for acute exposures to TNFα or product-conditioned medium after four days of seeding to ensure the stability of the tube formation. Longer treatments may show different mediator and gene expression profiles more representative of the chronic conditions that lead to the development of vascular disorders. However, evaluations of endothelial microvessel barrier stability for more than eight will be required before conducting longer exposures.

Other microfluidic systems have been developed to study the adhesion of blood cells, such as leukocytes (e.g., neutrophils), erythrocytes and platelets, and cancer cells to endothelial cells in hemodynamic flow.[53–57] Various systems offer the functionality to control shear stress applied on endothelial cells, which are still, however, grown as a 2D monolayer.[53–56] Interestingly, more advanced systems can be fabricated to incorporate a channel containing a stenotic structure for flow characterization[54] or to mimic in vivo microvasculature network for studying the complete adhesion to transmigration cascade.[57] Nevertheless, the format of these microfluidics remains low-throughput due to the complexity of producing and handling.[54,57] A major advantage of the OrganoPlate® over other microfluidic systems is its microtiter format, which enables growing 96 independent microvessels, providing throughput capacity for multiple-condition testing,

useful for drug screening and dose-response studies. Moreover, continuous flow perfusion of media through HCAEC microvessels using gravity leveling instead of pumps facilitates handling and reduces the risk of contamination. The absence of a pump that permits the application of flow with specific shear stress magnitude and profiles (e.g., pulsatile, oscillatory) can be perceived as a limitation of the system. However, the constant evolution of the OrganoPlate® functionality and design may resolve this issue in the future. The availability of a three-lane OrganoPlate® provides significant potential to extend our HCAEC microvessel model to explore further functional aspects of vascular biology and disorders simultaneously using a single model (e.g. transmigration of monocytes). The development of co-cultures from various tissues/organs, such as smooth muscle cells, neuronal cells, or epithelial cells, paves the way to a range of potential applications. Additional experimental setups such as concomitant exposure of leukocytes and endothelium to a treatment under flow offer the flexibility to investigate independent and combined contribution of both cellular types to a mechanism of interest. Moreover, perfusing human blood or serum/plasma and using endothelial cells from donors with atherosclerosis and cardiovascular disorders or donors of various ages provides an opportunity to screen a wider human population and may further contribute to the translatability of our 3D vasculature-on-a-chip model and advance its development as a precision medicine selection tool.

Conclusions

In the context of the 3Rs principle that encourages the community to create relevant in vitro alternatives that reduce animal use, we developed and optimized a 3D vasculature-on-a-chip model using the microfluidic OrganoPlate® to investigate the process of leukocyte adhesion to the lumen of primary disease-relevant HCAEC microvessels under flow. In addition to functional readouts, we measured various molecular endpoints using high-content imaging and

transcriptomics, providing mechanistic insights into the model. We demonstrated the applicability of the model for real-world research and development projects, such as systems toxicology-based risk assessment of products in vitro. The OrganoPlate® format and its design evolutions provide scalability and potential for extending the model to investigate additional mechanistic aspects of vascular diseases that would complement cardiovascular disease risk assessment and open a wide spectrum of applications in vascular biology research and beyond.

Conflict of interest

This publication contains original work. The authors CP, AL, DP, KB, RD, EG, NVI, MCP, and JH are employees of Philip Morris International. The authors BK, HL, TO, MV, AvdH, and JJ are or were employees of MIMETAS BV. These affiliations are declared. The OrganoPlate® is a registered trademark of MIMETAS BV.

Acknowledgements

Philip Morris International is the sole source of funding and sponsor of this research. We thank Pauline Betsch and Dr Remko van Vught for project management support, Didier Goedertier and Claudius Pak for generating the aqueous smoke/aerosol extracts, Dr Alain Sewer for preparing and submitting transcriptomics data to the Array Express repository database and Frederik Schavemaker for support with schematic illustrations. We also thank Dr Dean Meyer from Edanz Medical Writing (www.edanzediting.com/ac), for editing a draft of this manuscript.

References

1. Radeva, M. Y. & Waschke, J. Mind the gap: Mechanisms regulating the endothelial barrier. Acta Physiol (Oxf) 222, (2018).
2. Favero, G., Paganelli, C., Buffoli, B. & others. Endothelium and its alterations in cardiovascular diseases: Life style intervention. Biomed Res Int 8018, (2014).
3. Insull Jr., W. The pathology of atherosclerosis: Plaque development and plaque responses to medical treatment. Am J Med 122, S3–S14 (2009).
4. Burden, N., Chapman, K., Sewell, F. & others. Pioneering better science through the 3rs: An introduction to the national centre for the replacement, refinement, and reduction of animals in research (nc3rs). J Am Assoc Lab Anim Sci 54, 198–208 (2015).
5. Lee, J., Packard, R. R. & Hsiai, T. K. Blood flow modulation of vascular dynamics. Curr Opin Lipidol 26, 376–383 (2015).
6. Chatterjee, S. Endothelial mechanotransduction, redox signaling and the regulation of vascular inflammatory pathways. Front Physiol 9, 524 (2018).
7. Hsieh, H. J., Liu, C. A., Huang, B. & others. Shear-induced endothelial mechanotransduction: The interplay between reactive oxygen species (ros) and nitric oxide (no) and the pathophysiological implications. J Biomed Sci 21, 3 (2014).
8. van Duinen, V. et al. 96 perfusable blood vessels to study vascular permeability in vitro. Sci Rep 7, 18071 (2017).
9. Bogorad, M. I., DeStefano, J., Karlsson, J. & others. Review: In vitro microvessel models. Lab Chip 15, 4242–4255 (2015).
10. Nahrendorf, M. & Swirski, F. K. Lifestyle effects on hematopoiesis and atherosclerosis. Circ Res 116, 884–894 (2015).
11. Messner, B. & Bernhard, D. Smoking and cardiovascular disease: Mechanisms of endothelial dysfunction and early atherogenesis. Arterioscler Thromb Vasc Biol 34, 509–515 (2014).
12. Yanbaeva, D. G., Dentener, M. A., Creutzberg, E. C. & others. Systemic effects of smoking. Chest 131, 6–2179 (2007).
13. General, S. In (eds.), How tobacco smoke causes disease: The biology and behavioral basis for smoking-attributable disease: A report of the surgeon general. (2010).
14. Murphy, J., Gaca, M., Lowe, F. & others. Assessing modified risk tobacco and nicotine products: Description of the scientific framework and assessment of a closed modular electronic cigarette. Regul Toxicol Pharmacol 90, 342–357 (2017).
15. Food & Administration, D. Modified risk tobacco product applications: Draft guidance for industry. Http://www.Fda.Gov/downloads/tobaccoproducts/guidancecomplianceregulatoryinformation/ucm297751.Pdf (2012).
16. Schaller, J. P., Keller, D., Poget, L. & others. Evaluation of the tobacco heating system Part 2: Chemical composition, genotoxicity, cytotoxicity, and physical properties of the aerosol. Regul Toxicol Pharmacol 81, S27–S47 (2016).
17. Poussin, C., Laurent, A., Kondylis, A. & others. In vitro systems toxicology-based assessment of the potential modified risk tobacco product chtp for vascular inflammation- and cytotoxicity-associated mechanisms promoting adhesion of monocytic cells to human coronary arterial endothelial cells. Food Chem Toxicol 120, 390–406 (2018).
18. Poussin, C., Laurent, A., Peitsch, M. C., Hoeng, J. & De Leon, H. Systems toxicology-based assessment of the candidate modified risk tobacco product THS2.2 for the adhesion of monocytic cells to human coronary arterial endothelial cells. Toxicology 339, 73–86 (2016).
19. Phillips, B., Veljkovic, E., Boue, S. & others. An 8-month systems toxicology inhalation/cessation study in apoe-/- mice to investigate cardiovascular and respiratory exposure effects of a candidate modified risk tobacco product, ths , compared with conventional cigarettes. Toxicol Sci 149, 411–432 (2016).
20. van der Toorn, M. et al. Aerosol from a candidate modified risk tobacco product has

reduced effects on chemotaxis and transendothelial migration compared to combustion of conventional cigarettes. Food and Chemical Toxicology 86, 81–87 (2015).
21. Ludicke, F., Picavet, P., Baker, G. & others. Effects of switching to the menthol tobacco heating system smoking abstinence, or continued cigarette smoking on clinically relevant risk markers: A randomized, controlled, open-label, multicenter study in sequential confinement and ambulatory settings. Nicotine Tob Res 20, 173–182 (2018).
22. Fratta Pasini Anna AND Albiero, Serum Oxidative Stress-Induced Repression of Nrf2 and GSH Depletion: A Mechanism Potentially Involved in Endothelial Dysfunction of Young Smokers. PLoS One 7, 1–12 (2012).
23. Haralick, R. M., Sternberg, S. R. & Zhuang, X. Image analysis using mathematical morphology. IEEE Transactions on Pattern Analysis and Machine Intelligence PAMI- 9, 550–632 (1987).
24. Sternberg. Biomedical image processing. Computer (Long Beach Calif) 16, 22–34 (1983).
25. Lee, S. U., Chung, S. Y. & Park, R. H. A comparative performance study of several global thresholding techniques for segmentation: Computer Vision. Graphics, and Image Processing 52, 171–190 (1990).
26. Dai, M., Wang, P., Boyd, A. D. & others. Evolving gene/transcript definitions significantly alter the interpretation of genechip data. Nucleic Acids Res 33, 175 (2005).
27. McCall, M. N., Bolstad, B. M. & Irizarry, R. A. Frozen robust multiarray analysis (frma). Biostatistics 11, 242–253 (2010).
28. Bolstad, B. M. Quality assessment of affymetrix genechip data. in (eds (eds. r., G., carey v.J., huber w., irizarry r.A. & dudoit s.) (bioinformatics and computational biology solutions using r and bioconductor. Statistics for biology and health. Springer, 2005). doi:https://doi.org/10.1007/0-387-29362-0_3.
29. Smyth, G. K. Linear models and empirical bayes methods for assessing differential expression in microarray experiments. Stat Appl Genet Mol Biol 3, (2004).
30. Benjamini, Y. & Hochberg, Y. Controlling the false discovery rate: A practical and powerful approach to multiple testing: Journal of the Royal Statistical Society Series B 57. 289–300 (1995).
31. Martin, F., Sewer, A., Talikka, M. & others. Quantification of biological network perturbations for mechanistic insight and diagnostics using two-layer causal models. BMC Bioinformatics 15, 238 (2014).
32. sbv IMPROVER project team Ansari, S. B. J. et al. On crowd-verification of biological networks. 7, 307–325 (2013).
33. Boue, S., Talikka, M., Westra, J. W. & others. Causal biological network database: A comprehensive platform of causal biological network models focused on the pulmonary and vascular systems. Database (Oxford) 30, (2015).
34. Subramanian, A., Tamayo, P., Mootha, V. K. & others. Gene set enrichment analysis: A knowledge-based approach for interpreting genome-wide expression profiles. Proc Natl Acad Sci U S A 10, 15545–15550 (2005).
35. Ackermann, M. & Strimmer, K. A general modular framework for gene set enrichment analysis. BMC Bioinformatics 10, 47 (2009).
36. of Canada, G. Tobacco products information regulations. Https://www.Canada.Ca/en/health-canada/services/health-concerns/reports-publications/tobacco/tobacco-products-information-regulations.Html (2000).
37. Poussin, C., Laurent, A., Peitsch, M. C. & others. Systems biology reveals cigarette smoke-induced concentration-dependent direct and indirect mechanisms that promote monocyte-endothelial cell adhesion. Toxicol Sci 147, 370–385 (2015).
38. Granger, D. N. & Senchenkova, E. Inflammation and the microcirculation. (2010).
39. Grigoryan, H., Edmands, W., Lu, S. S. & others. Adductomics pipeline for untargeted analysis of modifications to cys34 of human serum albumin. Anal Chem 88, 10504–10512 (2016).
40. Vormann, M. K., Gijzen, L., Hutter, S. & others. Nephrotoxicity and kidney transport

assessment on 3d perfused proximal tubules. AAPS J 20, 90 (2018).
41. Cucullo, L., Hossain, M., Puvenna, V., Marchi, N. & Janigro, D. The role of shear stress in Blood-Brain Barrier endothelial physiology. BMC Neurosci 12, 40 (2011).
42. Imanaka-Yoshida, K. Extracellular matrix remodeling in vascular development and disease. Etiology and morphogenesis of congenital heart disease: from gene function and cellular interaction to morphology 221–226 (2016).
43. Muncie, J. M. & Weaver, V. M. The physical and biochemical properties of the extracellular matrix regulate cell fate. Curr Top Dev Biol 130, 1–37 (2018).
44. Mongiat, M., Andreuzzi, E., Tarticchio, G. & others. Extracellular matrix, a hard player in angiogenesis. Int J Mol Sci 17, (2016).
45. Chen, Y., Gu, J., Li, D. & others. Time-course network analysis reveals tnf-alpha can promote g1/s transition of cell cycle in vascular endothelial cells. Bioinformatics 28, 1–4 (2012).
46. Amberger, A., Maczek, C., Jurgens, G. & others. Co-expression of icam-1, vcam-1, elam-1 and hsp60 in human arterial and venous endothelial cells in response to cytokines and oxidized low-density lipoproteins. Cell Stress Chaperones 2 1, 94–103 (1997).
47. Jia, Z., Nallasamy, P., Liu, D. & others. Luteolin protects against vascular inflammation in mice and tnf-alpha-induced monocyte adhesion to endothelial cells via suppressing ikappabalpha/nf-kappab signaling pathway. J Nutr Biochem 26, 293–302 (2015).
48. Langert, K. A., Zee, V., L., C. & Stubbs Jr., B. Jr. S. E. Tumour necrosis factor alpha enhances ccl2 and icam-1 expression in peripheral nerve microvascular endoneurial endothelial cells. ASN Neuro 5, (2013).
49. Mulligan, M. S., Vaporciyan, A. A., Miyasaka, M. & others. Tumor necrosis factor alpha regulates in vivo intrapulmonary expression of icam-1. Am J Pathol 142, 1739–1749 (1993).
50. Zachlederova, M. & Jarolim, P. The dynamics of gene expression in human lung microvascular endothelial cells after stimulation with inflammatory cytokines. Physiol Res 55, 39–47 (2006).
51. Zhang, X., Wang, L., Zhang, H. & others. The effects of cigarette smoke extract on the endothelial production of soluble intercellular adhesion molecule-1 are mediated through macrophages, possibly by inducing tnf-alpha release. Methods Find Exp Clin Pharmacol 24, 261–265 (2002).
52. Rennert, K., Heisig, K., Groeger, M. & others. Recruitment of cd16(+) monocytes to endothelial cells in response to lps-treatment and concomitant tnf release is regulated by cx3cr1 and interfered by soluble fractalkine. Cytokine 83, 41–52 (2016).
53. Conant, C. G., Schwartz, M. A., Nevill, T. & others. Platelet adhesion and aggregation under flow using microfluidic flow cells. vol. 2009 (J Vis Exp).
54. Lee, J., Huh, H. K., Park, S. H. & others. Endothelial cell monolayer-based microfluidic systems mimicking complex in vivo microenvironments for the study of leukocyte dynamics in inflamed blood vessels. Methods Cell Biol 146, 23–42 (2018).
55. Thompson, T. J. & Han, B. Analysis of adhesion kinetics of cancer cells on inflamed endothelium using a microfluidic platform. Biomicrofluidics 12, 42215 (2018).
56. White, J., Lancelot, M., Sarnaik, S. & others. Increased erythrocyte adhesion to vcam-1 during pulsatile flow: Application of a microfluidic flow adhesion bioassay. Clin Hemorheol Microcirc 60, 201–213 (2015).
57. Lamberti, G., Prabhakarpandian, B., Garson, C. & others. Bioinspired microfluidic assay for in vitro modeling of leukocyte-endothelium interactions. Anal Chem 86, 8344–8351 (2014).

Supplementary materials

The supplementary tables were not printed due to the length, they are available for download in the orgininal manuscript:
10.14573/altex.1811301

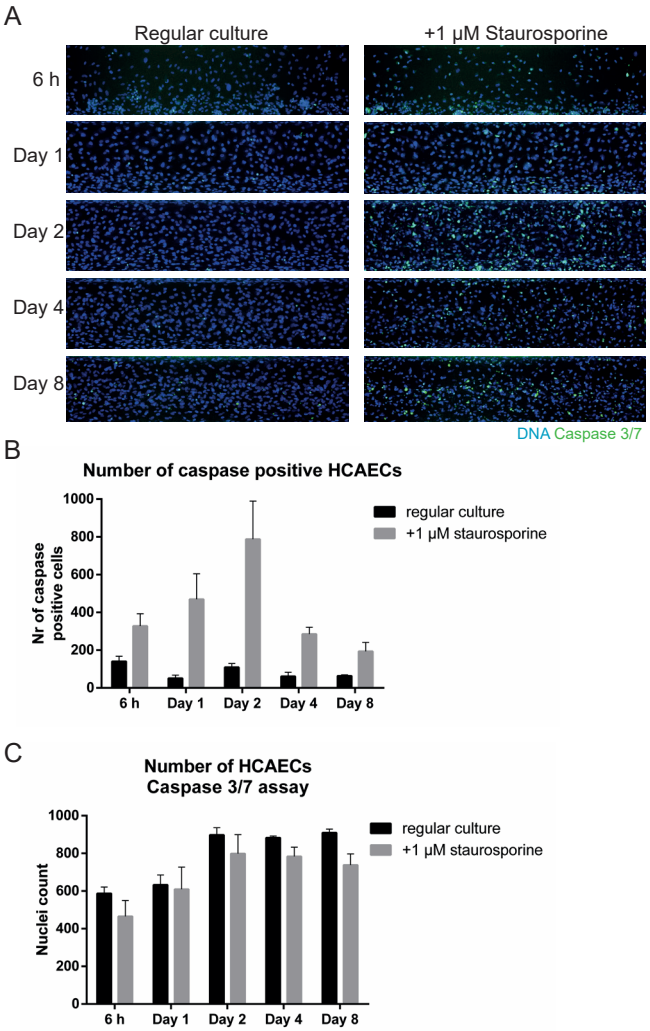

Supplementary figure 1. Quantification of caspase 3/7 activity in HCAEC microvessels up to 8 days culture. (A) HCAEC microvessels were stained for caspase 3/7 at different time points during regular culture (left) or after a 2hour-incubation with 1 µM staurosporine. **(B)** Quantification of the number of caspase 3/7 positive HCAEC cells (N=1, n = 4). **(C)** Quantification of the total number of HCAEC nuclei (N=1, n = 4). Bars represent average + standard deviation. No statistical analysis given N=1.

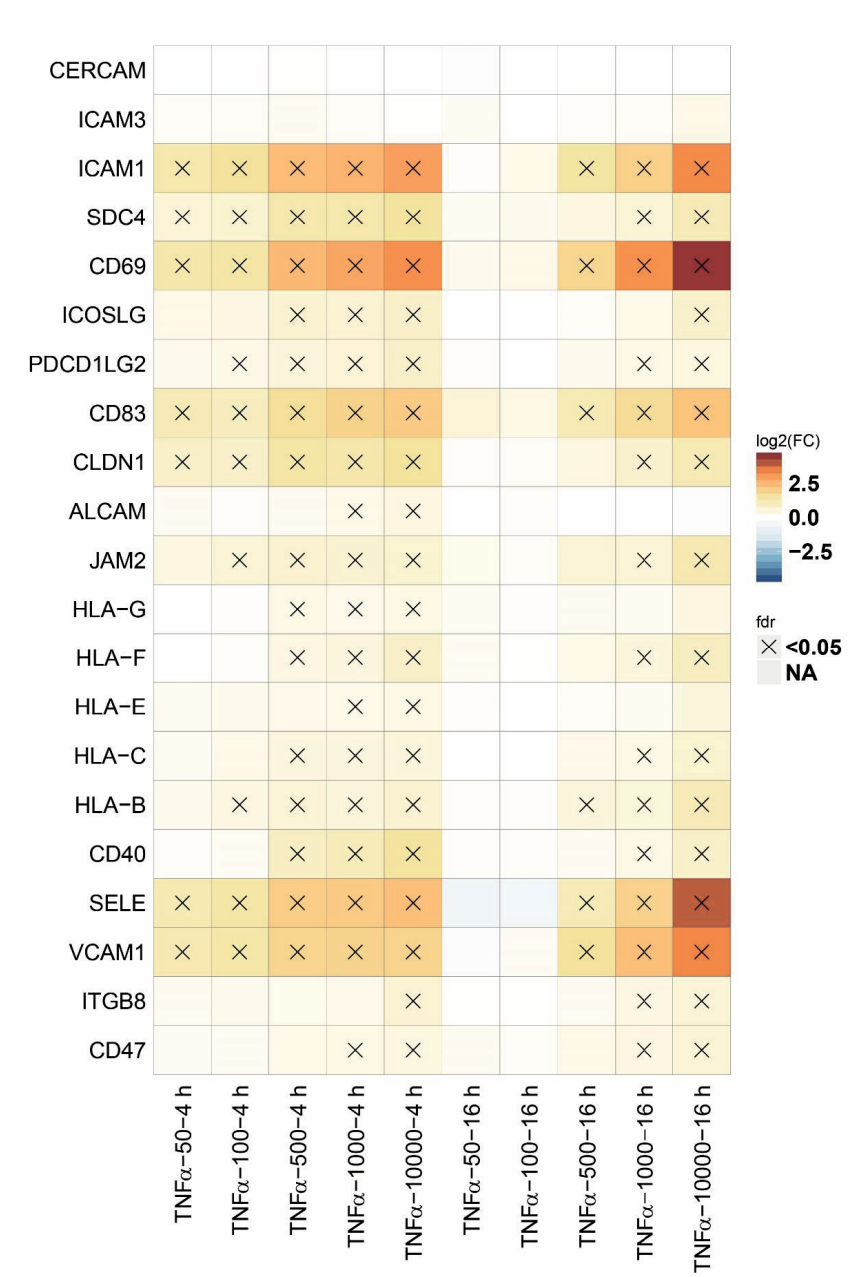

Supplementary Figure 2. The FC of mRNA transcripts coding for adhesion molecules in HCAEC microvessels treated with TNFα for four and 16 hours. Heatmap of adhesion molecule-encoding gene expression FCs (as a log2 scale) comparing the effect of TNFα relative to VC. The symbol "X" in the heatmap indicates that the FC is statistically significant (FDR ≤ 0.05). Abbreviations: h, hours.

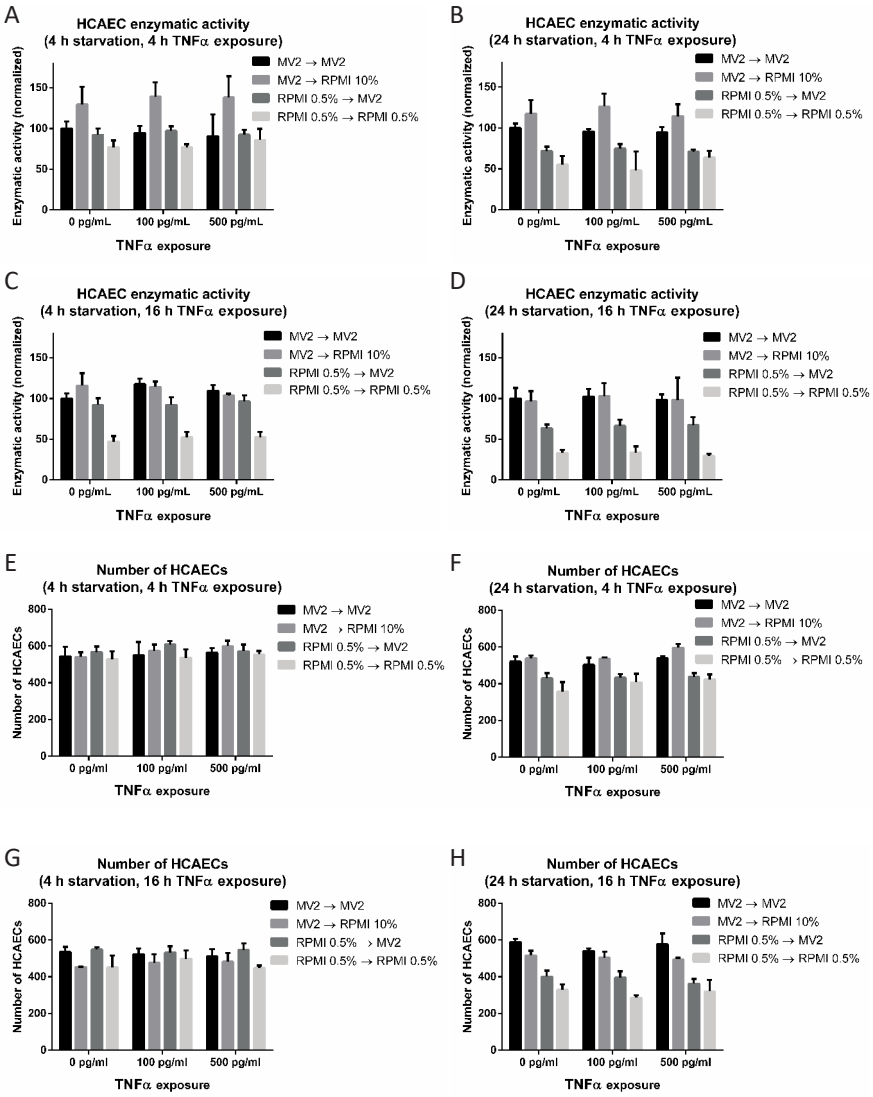

Supplementary Figure 3. Effect of serum content in medium on the viability and number of HCAECs in microvessels. The viability and number of HCAECs within microvessels was assessed using the WST-8 enzymatic assay **(A – D)** and counting Hoechst-stained nuclei **(E – H)**, respectively, after four and 24 hours exposure to low (0.5%) or normal (5%) serum content in culture medium followed by four or 16 hours exposure to TNFα diluted in low (0.5%), normal (5%) and high (10%) serum content after medium change as illustrated by an arrow. WST-8 absorbance was measured 30 minutes after the addition of the reagent. RPMI medium was supplemented with 0.5% or 10% fetal bovine serum. Bars represent the mean + standard deviation and all WST-8 enzymatic activity values are normalized to the MV2 0 pg/mL TNFα condition. N= 1 independent experiment, n = 3 - 5. Abbreviations: h, hours.

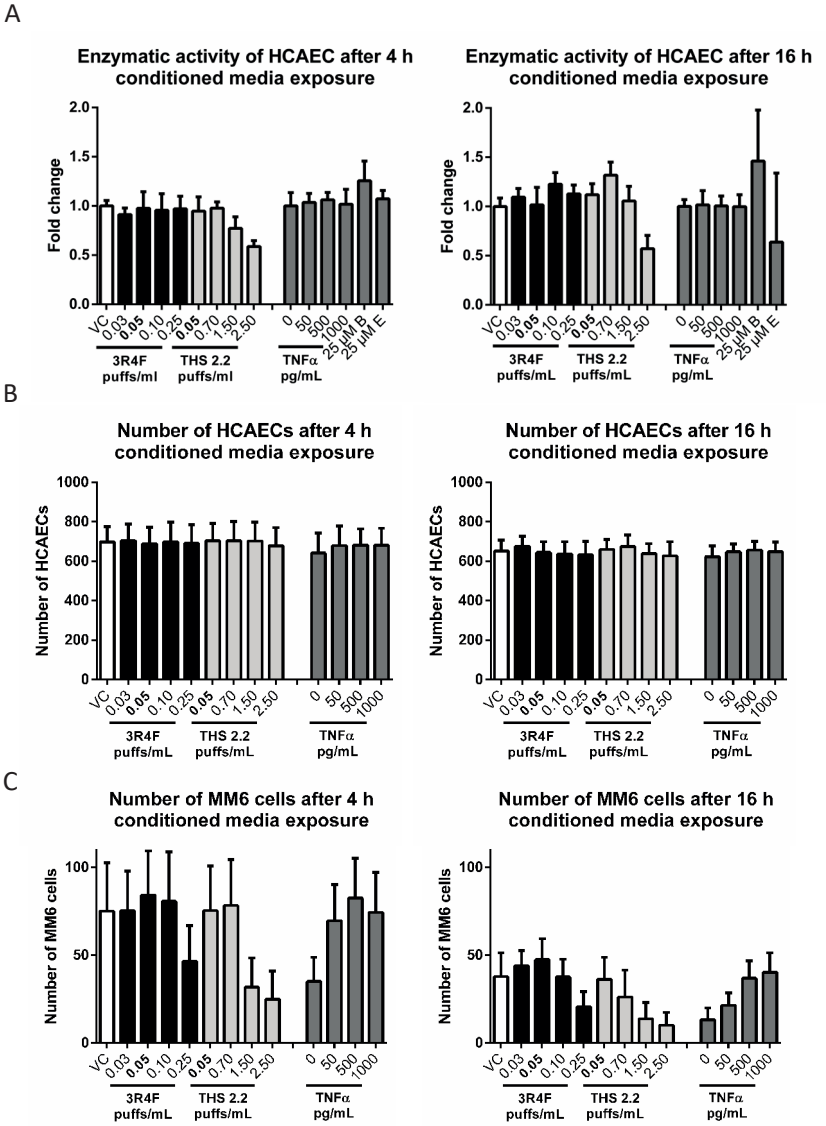

Supplementary Figure 4: Effect of 3R4F- and THS 2.2-conditioned media on the viability and number of HCAECs in microvessels (A) The viability and proliferation of HCAECs forming the microvessels was assessed using the WST-8 enzymatic assay after 4 and 16 h of conditioned medium exposure. WST-8 absorbance was measured 30 min after addition of the reagent (N = 2, n = 3). Data are expressed as fold change relative to the vehicle control (VC) corresponding to conditioned medium with 0 puffs/ml of aqueous extract from 3R4F smoke or THS2.2 aerosol. **(B)** Hoechst-stained nucleus counts and MM6 **(C)** in HCAEC microvessels after 4 and 16 h of conditioned medium exposure. Bars represent the mean + SD. N = 4, n = 4-6. 3R4F, reference cigarette; THS 2.2, Tobacco Heating System 2.2; B, L-buthionine-sulfoximine; E, ethacrynic acid.